Place-cell heterogeneity underlies power laws in coarse-grained hippocampal activity

J. J. Briguglio,[1] J. Lee,[1,2] A. K. Lee,[1,2] V. Hakim,[1,3,*] and S. Romani[1,†]

[1]*Janelia Research Campus, 19700 Helix Drive, Ashburn, Virginia 20147, USA*

[2]*Howard Hughes Medical Institute, Beth Israel Deaconess Medical Center, 330 Brookline Avenue, Boston, Massachusetts 02215, USA*

[3]*Laboratoire de Physique de l'École Normale Supérieure, CNRS, École Normale Supérieure, PSL University, Sorbonne Université, Université Paris Cité, Paris, France*

(Received 2 October 2025; accepted 9 September 2026; published 4 November 2026)

Power-law scaling in coarse-grained data has been linked to critical dynamics, but the true source of this scaling often remains unclear. Here, we analyze neural activity recorded during spatial navigation, reproducing power-law scaling under a phenomenological renormalization group (PRG) procedure that clusters units by activity similarity. Such scaling was previously characterized as describing a nontrivial fixed point. We show that the iterative nature of the procedure itself leads to the emergence of power laws when applied to a noncritical model consisting of heterogeneous, noninteracting units obeying spatially structured activity. Furthermore, the scaling exponents produced by heterogeneous noninteracting units match the observed exponents in recorded neural data. A simplified version of the PRG further reveals how heterogeneity smooths transitions across scales in our model, mimicking critical behavior. The resulting exponents depend systematically on system and population size, predictions confirmed by subsampling the data, further distinguishing these effective PRG exponents from true critical exponents.

DOI: 10.1103/hvk8-9hl2

I. INTRODUCTION

Renormalization group (RG) techniques probe interacting systems for power-law scaling, revealing critical phenomena [1–4]. Inspired by RG, coarse-graining methods applied to empirical data can extract critical exponents to classify system dynamics [5–9], yet power laws can also stem from noncritical processes, obscuring interpretation when system details are limited [10–18]. This ambiguity complicates analyzing empirical datasets, including those from biological systems, where coarse graining often suggests critical states [6,19,20].

Recent studies applying a phenomenological renormalization group (PRG) to neural activity from mice navigating spatially have reported power-law scaling, suggesting nontrivial fixed points [5,6]. So far, traditional models of spatially tuned units have failed to replicate this scaling [5,16], fueling debate over the underlying mechanisms [12,15,20,21]. As an alternative explanation to the existence of a critical point in the renormalization group sense, the appearance of approximate power laws has been attributed to the existence of fluctuating global variables [10–12,16,18]. Along this line, a tentative explanation of the results of Ref. [6] was proposed [16] by postulating the existence of several ($\geqslant$5) temporally fluctuating latent variables such as attention. In the absence of clear experimentally supported mechanisms, the origin of the power laws observed in Ref. [6] has, however, remained unclear.

Here, we construct a null model using data from a large spatial environment (40 m), where hippocampal CA1 neurons exhibit striking heterogeneity in place-field distributions that can be modeled as independent Poisson processes with Gamma-distributed rates [22,23], lacking any interactions between neurons that could underlie criticality. After reproducing previous findings, we demonstrate that this heterogeneous, independent model alone generates the observed scaling under PRG, producing power laws that mimic signatures of criticality. Importantly, this model is only based on the experimentally well-documented heterogeneity of hippocampal cell place fields. This reveals that PRG can transform unit-level variability into a limited form of scale invariance characterized by effective rather than true exponents, reshaping power-law interpretations across complex systems.

II. RESULTS

Transgenic mice ($n = 4$) expressing GCaMP6f were trained to run on a spherical treadmill (40 cm diameter) in multiple 40-m-long virtual environments [Fig. 1(a)]. Water rewards were provided randomly throughout the environment and the animals were "teleported" to the start after running the entire length of the track. Calcium activity of dorsal hippocampal CA1 pyramidal neurons was imaged, yielding 700–870 neurons per session [Fig. 1(b)]. In each session, the animals ran eight laps in a single familiar environment. Calcium signals were filtered and normalized to yield binary signals representing when a cell was active [Fig. 1(c)]. Additional experimental and data preprocessing details are presented in Ref. [23].

*Contact author: vincent.hakim@phys.ens.fr

†Contact author: romanis@janelia.hhmi.org

Published by the American Physical Society under the terms of the Creative Commons Attribution 4.0 International license. Further distribution of this work must maintain attribution to the author(s) and the published article's title, journal citation, and DOI.

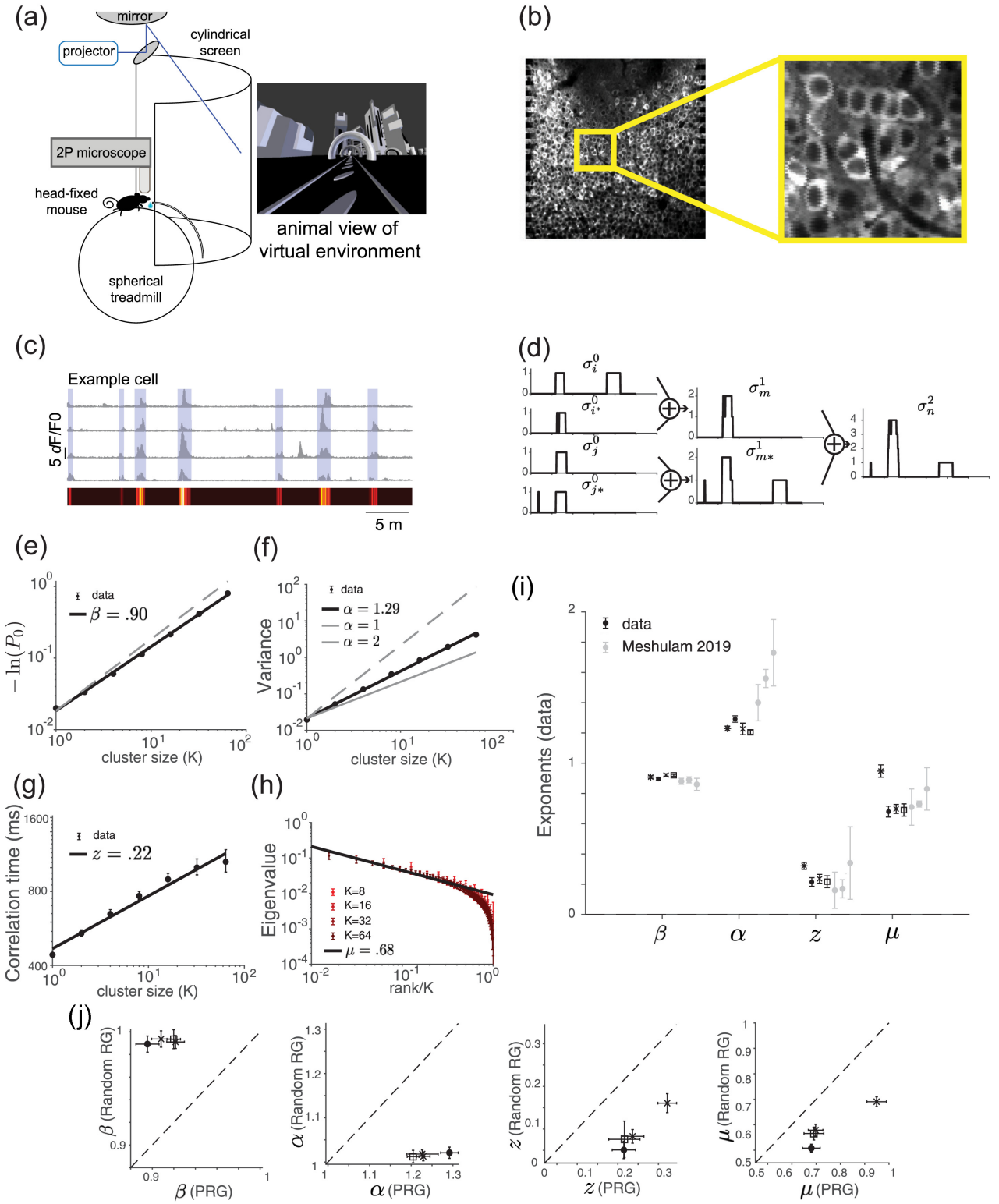


FIG. 1. Experimental schematic. (a) A transgenic mouse runs on a spherical treadmill that moves the animal through a virtual environment projected onto a surrounding screen. (b) Hippocampal cells are viewed via calcium imaging, giving hundreds of cells per recording. (c) An example cell exhibits peaks in calcium response consistently across laps in multiple locations. (d) Phenomenological renormalization group procedure is performed on binarized versions of the single-cell signals by combining cells with most correlated activity in a recursive fashion. This produces power-law scaling for (e) negative logarithm of the probability of silence, (f) variance, (g) correlation time, and (h) within-cluster eigenvalue spectrum. Power-law scaling exponents across mice are summarized in panel (i) (95% confidence intervals), with each marker representing a different mouse. (j) Comparison of measured exponents under maximal-pair combining (PRG) and random-pair combining (random RG, 95% confidence intervals).

The binarized activity traces from N recorded neurons, $\sigma_i^0(t)$, $i = 1, \ldots, N$, were used as the inputs to the PRG analysis used in Ref. [6]. Briefly, coarse graining was achieved by constructing units at level $k+1$ starting with a pool of all units at level k. The pair of units at coarse-graining level k with the maximal correlation between their activity traces was chosen and their activity summed. The resultant trace was placed as a single unit at level $k+1$, and the selected pair was removed from the pool at level k. The procedure was iterated until no pairs were left at level k. The procedure is initiated with single neuron activity, leading to a first coarse-grained set of units $\sigma_i^1(t)$, $i = 1, \ldots, \lfloor N/2 \rfloor$. This process was repeated as long as there remained at least $N_{\min} = 4$ units, summing the activity traces of all paired units at each stage [Fig. 1(d)]. After k iterations, the activity of each of the $N_k = \lfloor N/2^k \rfloor$ units $\sigma_i^k(t)$ was a sum of the activity of a cluster of $K = 2^k$ recorded neurons. At each step, the probability of silence ($P_0(k) = \langle P(\sigma_i^k(t) = 0)\rangle_{N_k,t}$), the mean variance of individual units ($\mathrm{Var}(K) = \langle\langle \sigma_i^k(t)^2\rangle_t - \langle \sigma_i^k(t)\rangle_t^2\rangle_{N_k}$), the correlation time ($\tau_{\mathrm{corr}}(K)$ exponential timescale fit to the average autocorrelation function $\langle R_{\sigma_i^k\sigma_i^k}(\Delta t)\rangle_{N_k}$), and the within-cluster eigenvalue spectra are computed. The within-cluster eigenvalue spectrum is $\lambda_r(K) = \langle \mathrm{Eigv}(C(m,k), r)\rangle_{N_k}$, where $\mathrm{Eigv}(X, r)$ returns the rth largest eigenvalue of matrix X. The matrix $C(m,k)$ is the covariance matrix of the units that comprise the mth coarse-grained unit at the kth PRG iteration i.e., the $\sigma_{i_m}^0$, with $\sum_{i_m} \sigma_{i_m}^0 = \sigma_m^k$. Three exponents are computed by fitting a first-order polynomial to the log-transformed relationships described by $\mathrm{Var} \propto K^\alpha$, $-\ln(P_0) \propto K^\beta$, and $\tau_{\mathrm{corr}} \propto K^z$. The within-cluster eigenvalue spectrum was fit to the relationship $\lambda_r = A(K/r)^\mu$, where λ_r denotes the rth largest eigenvalue (see Refs. [5,6]). We used a first-order polynomial fit to the corresponding log-transformed relationship on the four largest K values per session excluding $r/K > 0.5$ in order to capture the scaling of the larger eigenvalues, rather than the bulk of low eigenvalues, as expected for these matrices (see Ref. [24]).

We sought to reproduce the power-law scaling observed following the application of the PRG procedure to hippocampal CA1 data. Silence probability, variance, correlation time, and eigenvalue spectrum were each well described by power laws [Figs. 1(e)–1(h)]. We noted consistency in the power-law exponents across mice [Fig. 1(i), black markers]. This analysis qualitatively reproduces previous findings [5,6], though we observed systematic differences relative to previously reported values, most noticeably in the exponent associated with the scaling of the variance [Fig. 1(i), compare black with gray markers].

To establish the significance of these results, we first built a simple control coarse-graining procedure that pairs neurons randomly (random PRG), rather than based on their activity correlation. Using this procedure, we observed power-law scaling behavior with trivial scaling exponents for $\alpha \approx 1$ and $\beta \approx 1$, as expected for sums of independent binary units. These control exponents are far from those resulting from the PRG procedure [Fig. 1(j)]. We similarly observed different values for z and μ relative to our control. This demonstrates that the correlation structure in the data gives rise to nontrivial exponents (Fig. 1).

We next considered the possible contribution of spatially tuned firing, a hallmark of hippocampal activity, to the power laws observed with the application of the PRG procedure. We used an accurate statistical model of CA1 place-field activity, composed of model neurons with independent (conditionally on spatial location), heterogeneous, reliable place fields [Fig. 2(a)] [22,23]. The probability of neuron i having a field in some region was defined as a Poisson process, $P_i(x) = 1 - e^{(-\rho_i \Delta x)}$, where x denotes the spatial bin of size $\Delta x = 1$ cm. The Poisson rate ρ_i was heterogeneous across cells, following a Gamma distribution $G(\rho; a, b) = b^a \rho^{a-1} e^{-b\rho}/\Gamma(a)$ with shape parameter a and rate parameter b, both fit to maximize the likelihood of observing the measured field number distribution [23]. Each simulated neuron had a modeled calcium spike rate described by $R_i(x(t)) = B + A\sum_k \exp[-(x(t) - x_k^{(i)})^2/2s^2]$, where B is a background transient rate, A is the peak amplitude of the place fields, $x_k^{(i)}$ denotes the field locations for unit i, $\sum_k$ sums over all place fields, and $s = 10$ cm determines the field size (chosen because it is similar to the typical observed field size). The field amplitude A and the background rate B were fit to match the measured population transient numbers using simulations over parameter ranges and choosing the best match. We simulated an animal running through the environment at a constant speed ($v = 30$ cm/s), $x(t) = vt$, and generated calcium spikes (sampled at 30 Hz) as a Poisson process with rate based on the animal's location at each time. To mimic calcium transient durations measured from our imaging recordings, each calcium spike was replaced by a signal of constant amplitude for a duration T beginning at the simulated spike time, sampled from the exponential distribution $P(T) = 1/T^* e^{(-T/T^*)}$ (the characteristic shape we observed in the data), where T^* was the average transient duration (i.e., the maximum-likelihood estimate) estimated from the recordings, separately for each session [Fig. 2(a)]. The fit parameters are presented in Table I.

The simulated data were then analyzed in the same manner as the measured empirical data. We observed power-law scaling for the silence probability [Fig. 2(b)], the variance [Fig. 2(c)], the correlation time [Fig. 2(d)], and the eigenvalue spectra [Fig. 2(e)]. Additionally, the corresponding exponents are consistent with those derived from the empirical data [Fig. 2(f)]. Hence, a model with independent neurons, whose correlations solely arise from spatial coding, could reproduce the power-law scaling exponents extracted from the data.

We next sought to understand how this model could give rise to power laws. We constructed an approximate PRG procedure based on a simplified model of spatial coding neurons

TABLE I. Heterogeneous model parameters fit for each animal. a and b are the shape and rate parameters, respectively, for the Gamma distribution describing heterogeneous field formation. A and B are the amplitudes of the spatially modulated and background calcium transient rates, respectively. T^* is the exponential timescale describing each animal's observed transient durations.

Mouse	a	b (environment/field)	A (Hz)	B (Hz)	T^* (30 Hz bins)
1	0.443	0.226	2.00	0.0020	11.0
2	2.37	0.969	2.75	0.0070	14.3
3	0.855	0.254	2.00	0.0030	11.7
4	0.805	0.575	2.25	0.010	11.1

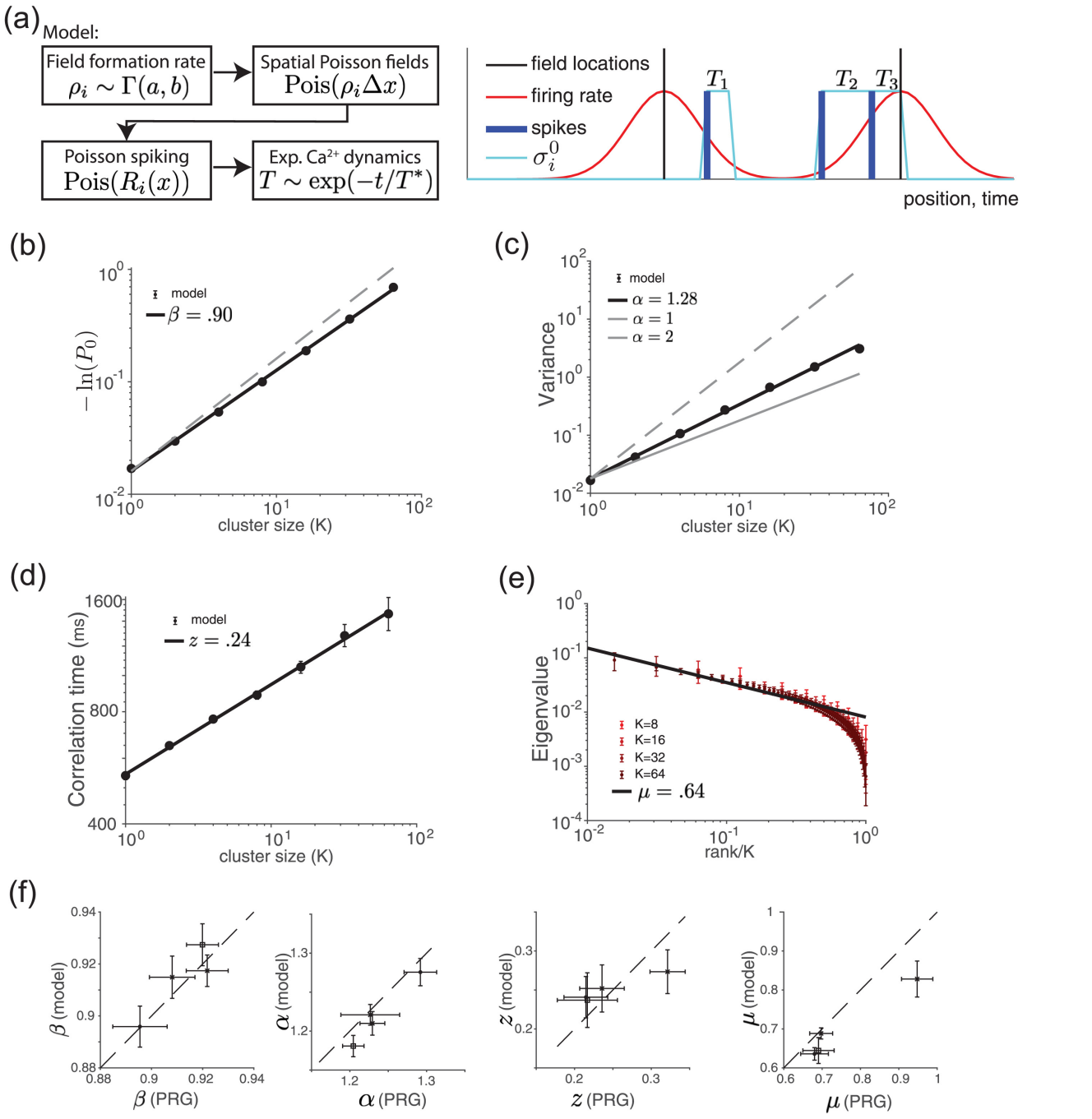


FIG. 2. Hippocampal spatial coding model recapitulates measured exponents. (a) Schematic of spatial coding model using parameters derived from experimental data. Power-law scaling is observed for (b) negative logarithm of the probability of silence, (c) variance, (d) autocorrelation time, and (e) within-cluster eigenvalue spectrum. (f) Comparison between exponents measured from hippocampal spatial coding model and directly from the data across animals (95% confidence intervals).

consisting of a population of binary place cells whose fields tile the environment. We first consider a model with homogeneous fields that are binary with size l and that uniformly tile the environment (field center of unit i is $x_i = Li/N$ with total environment size L and population size N). The activity of unit i without any coarse graining (iteration $k = 0$) is $\sigma_i^0(x) = \Theta(l/2 - |x - x_i|)$, where Θ is the Heaviside function (1 when the argument is positive, 0 otherwise) and x is the position of the simulated animal. In this model, units with adjacent place fields are the most correlated. Therefore, the coarse-graining procedure is simply defined as summing the activity of pairs of neighboring units at every iteration [Fig. 3(a)]. As shown below, this homogeneous tile model exhibits nonuniform power-law scaling with coarse graining. For example, if $1 \ll N_{\mathrm{active}} = Nl/L \ll N$, $\alpha \approx 2$ when $K \ll N_{\mathrm{active}}$ and $\alpha \approx 1$ when $N_{\mathrm{active}} \ll K \ll N$. Nonetheless, it

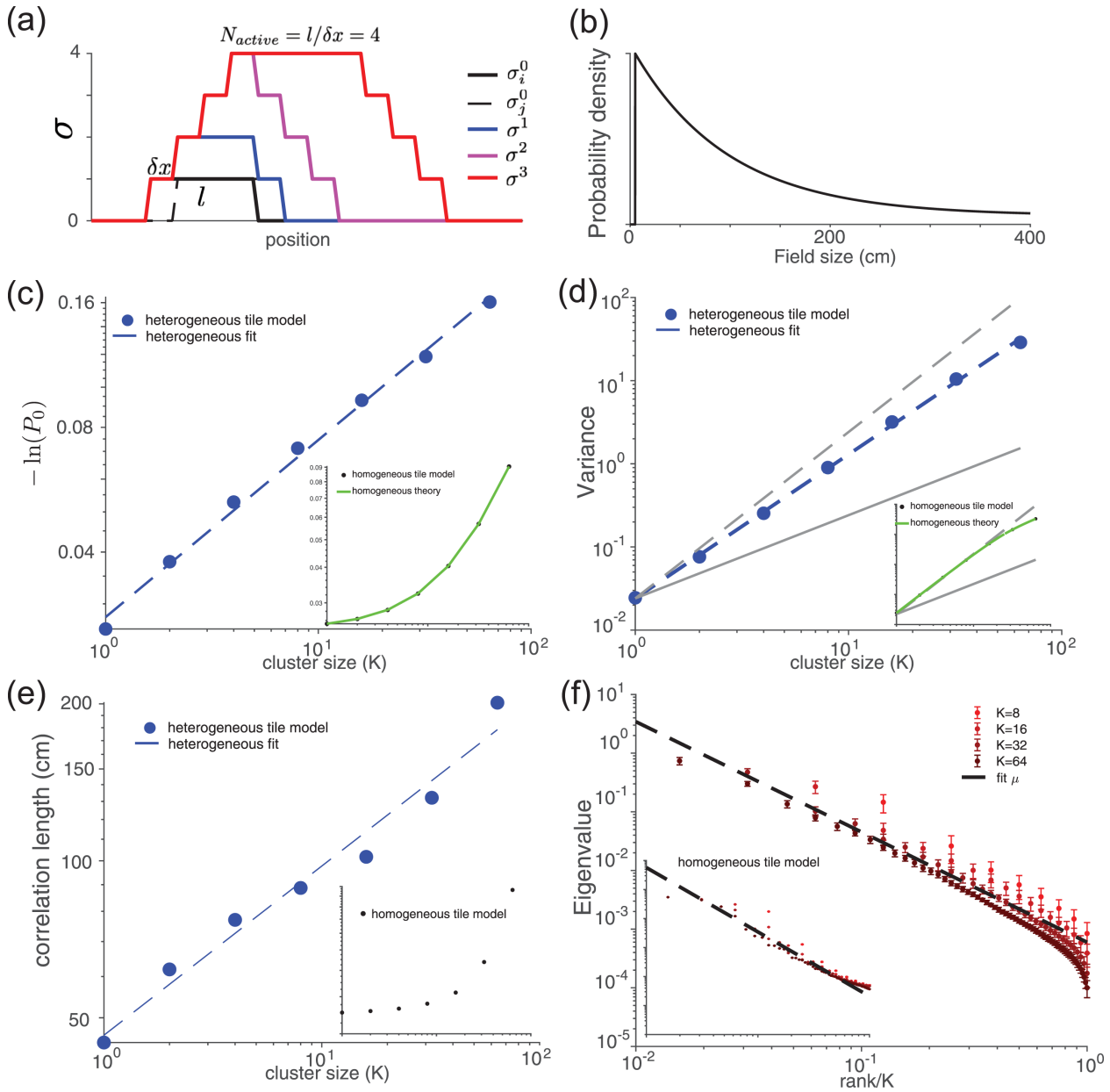


FIG. 3. Simplified spatial coding model. (a) Individual unit responses as coarse graining progresses show a distinct change in character around $K = N_{\text{active}}$. Significant heterogeneities in spatial response size [panel (b)] lead to apparent power-law scaling not visible in the homogeneous model (insets) for (c) negative logarithm of the probability of silence, (d) variance, (e) spatial autocorrelation length, and (f) within-cluster eigenvalue spectrum.

provides useful insights into the properties of a system where correlations are solely due to spatial tuning of the individual neurons. Note that the approximate PRG is similar in spirit to simple models that were previously proposed to describe the scaling properties of coarsening breath figures [25].

We simulated this homogeneous tile model using parameters approximating the reference data (environment size 40 m, field size 1 m, population size 1024) with an animal running at constant speed (30 cm/s) and used the PRG method described above. We observe that the probability of silence [Fig. 3(c), inset], variance [Fig. 3(d), inset], correlation length [Fig. 3(e), inset], and eigenvalue spectrum [Fig. 3(f), inset] do not follow an exact power-law scaling. Similar findings were obtained with the exact coarse graining described (shown) and with PRG using random permutations to break correlation symmetry (not shown). A mathematical analysis of this model (see Appendix) shows the presence of nonuniform scaling properties, determined by the number of units active at any given location, $N_{\text{active}} = l/\delta x$, where $\delta x = L/N$ is the spacing between neighboring units ($N_{\text{active}} = 25.6$ for the chosen parameters). A transition in scaling properties occurs at cluster size $K^* = N_{\text{active}}$, where coarse-grained units' field amplitudes continue to increase for $K < N_{\text{active}}$ and only field width increases for $K > N_{\text{active}}$. For instance, the variance, $\text{Var}(\sigma^K) = \sum_{i=0}^{3} a_i(K) K^i$, has different coefficients $a_i(K)$ for $K > N_{\text{active}}$ and $K < N_{\text{active}}$. Our analysis perfectly predicts the scaling properties for the probability of silence and variance [Figs. 3(c) and 3(d), insets]. We did not derive a closed-form

expression for the correlation length and eigenvalue spectrum, but the simulated results do not exhibit power-law scaling [Figs. 3(e) and 3(f), insets].

The most salient difference between the simple homogeneous tile model described above and our hippocampal place-field simulation (Fig. 2), and previous studies [5,16], is the presence of heterogeneity in spatial coding across neurons, which can be best quantified in large environments [23]. We explored the effect of such heterogeneity by considering a heterogeneous tile model in which the fields are drawn according to a Gamma distribution plus a constant minimum field size [Fig. 3(b)], $l_0 + l_r G(a_r, b_r)$, with $l_0 = 5\,\text{cm}$, $l_r = 95\,\text{cm}$, $a_r = 1$, and $b_r = 1$. These values of a_r and b_r are similar to those observed in mice recordings and are chosen for simplicity since the Gamma distribution simply reduces to an exponential distribution. When fit using the same methods as in the data, we observed scaling more closely matched to a power law for the probability of silence [Fig. 3(c)], variance [Fig. 3(d)], correlation length [Fig. 3(e)], and eigenvalue spectrum [Fig. 3(f)]. This is likely due to the heterogeneous length scales across neurons effectively smoothing out the transition in the homogeneous model. These results show how apparent scale invariance can appear in a simple place-cell model in the presence of heterogeneities.

We next used this heterogeneous tile model to explore whether differences in the measured exponents between this and previous studies [6] could be due to differences in the number of recorded neurons (fewer in this study) and/or environment size (larger in this study). When varying the population size, we observed that with a larger population size β and z decreased while α and μ increased [Fig. 4(a)]. When we varied environment size, we observed that increasing the environment size resulted in an increase of β, an inverted "u"-shaped curve for z, and a decrease of α and μ [Fig. 4(b)]. Hence, we find that differences in neural population and environment size could at least partially account for the differences between the exponents reported previously [6] and those measured in our data [Fig. 1(i)].

The strong dependence of the power-law exponents from the tile model on both environment and population size led us to reexamine our data and detailed place-field model. We reasoned that a procedure moving toward a nontrivial fixed point should exhibit power-law scaling and exponents that do not depend on these details. Therefore, we sought to quantify the effect of changing these parameters on the exponents estimated from the data by analyzing hippocampal responses using either smaller sections of the track or smaller numbers of recorded neurons. Decreasing population size [Fig. 4(c)] increased β and decreased α, produced small changes in z, and had inconsistent effects on μ across mice, but always produced small changes. Reducing environment size [Fig. 4(d)] increased α and μ while decreasing β, with an inverted "u" shape for z. This is largely consistent with the predictions from the simple heterogeneous tile model [Figs. 4(a) and 4(b)]. Moreover, the dependency of all of the exponents on population and environment size was well captured by our detailed model [Figs. 4(c) and 4(d), magenta curves]. These results provide evidence against the hypothesis that power-law scaling observed in hippocampal data under PRG results from critical exponents associated with a nontrivial fixed point.

III. DISCUSSION

Our analysis of spatial coding models reveals that population heterogeneity alone can produce power-law scaling under PRG with independent units. In the simplified tile model, power-law scaling is not uniform across scales: The homogeneous version exhibits two distinct regimes separated by the characteristic scale N_{active}, while heterogeneity smooths this transition into apparent power-law behavior over the experimentally accessible range. This effective scale invariance is distinct from the uniform scaling expected near a nontrivial fixed point. Moreover, our model predicts that the exponents depend systematically on population size and environment size, a dependence we confirmed in the data and one that is inconsistent with the interpretation of fixed-point exponents, with the general caveat that neural data only allows for a limited number of coarse-graining steps. Differences in these parameters also account for discrepancies between our measured exponents and those of previous studies. Overall, the power-law scaling observed in hippocampal data under PRG likely reflects known heterogeneities in place-cell coding rather than critical dynamics, although critical dynamics cannot be precluded by this analysis.

Previous models of place cells [6,16] relied on data taken in small environments where place cells typically exhibit one field with relatively small variation in place-field size. We demonstrated analytically that such homogeneous populations fail to produce power laws because two length scales emerge: the environment size L and the place-field size l. The resulting characteristic count, $N_{\text{active}} = Nl/L = l/\delta x$, creates distinct scaling regimes for cluster sizes $K \ll N_{\text{active}}$ versus $N \gg K \gg N_{\text{active}}$, with the variance scaling as K^2 and K^1, respectively [Eq. (A4)]. The experimentally accessible range of K sits between these asymptotes, where fitting yields effective exponents between the trivial limiting values. In the heterogeneous tile model, each neuron contributes a different characteristic scale, smearing the crossover into approximate power-law behavior. Although we used heterogeneity in place-field size to achieve this smoothing in the tile model, our biological model used a more realistic heterogeneity in hippocampal CA1 place-field number [22,23], achieving exponents that more closely match experiment. This means that the PRG analysis is a weak test of the presence of direct neuron-neuron interactions and does not indicate interactions are absent between these neurons. Interestingly, an accurate characterization of this heterogeneity emerges [26] from models with random projections from CA3 to CA1 hippocampal areas.

The previously proposed explanation for the emergence of power laws in the PRG procedure based on temporally fluctuating latent variables [16] can be revisited in the light of our results. Indeed, heterogeneous fluctuations of place-cell activities arise in our model from the "latent" motion of mice in space. However, in contrast to Ref. [16] where the existence of place cells plays no significant role, our model makes crucial use of the well-characterized heterogeneity of CA1 place fields and replaces an uncharacterized collection of latent fields by the uncontroversial mouse position.

The scaling we observe can be described as a generic, finite-range form of scale invariance [12], consistent with

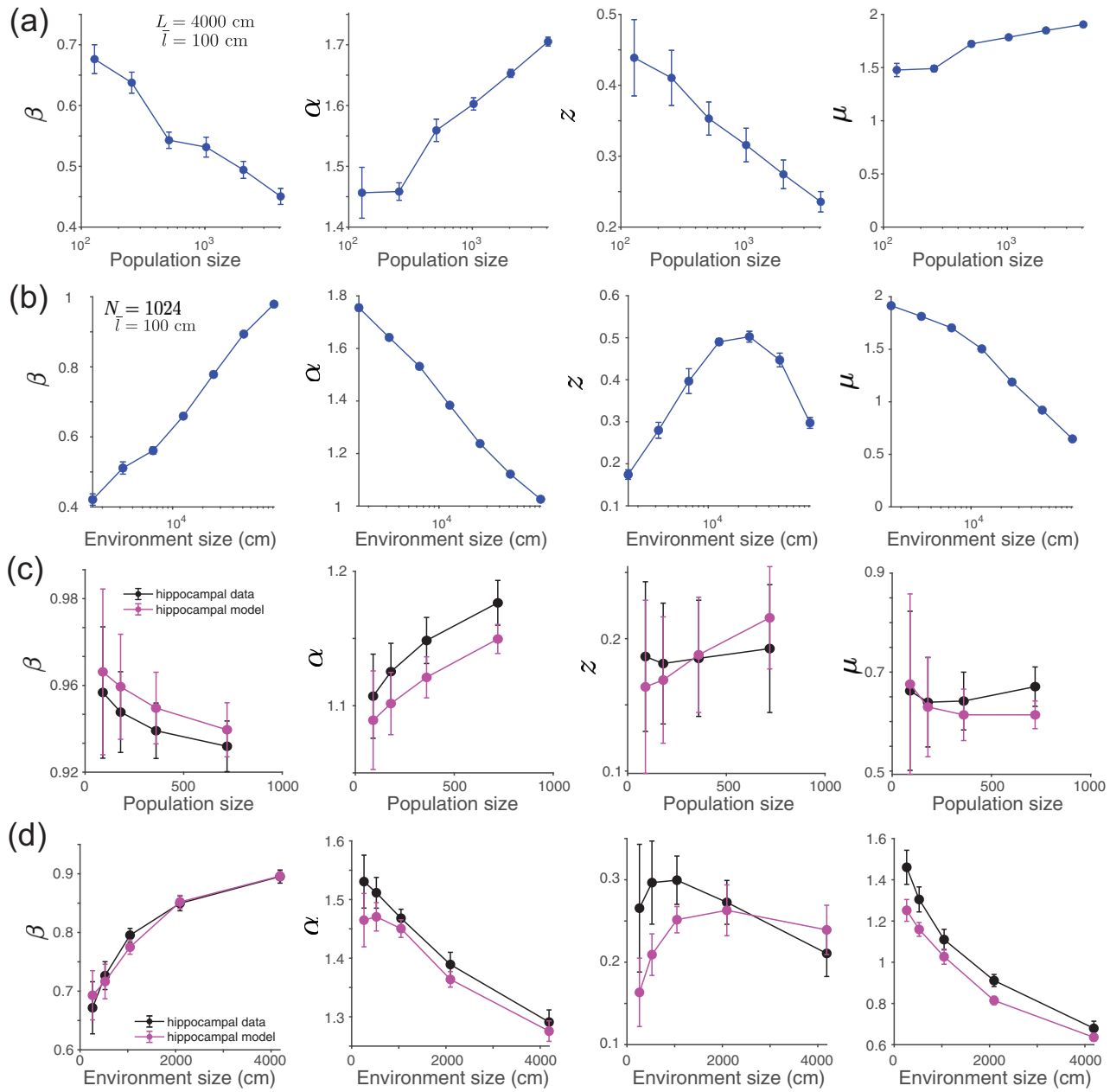


FIG. 4. Varying experimental parameters changes measured exponents. Changing the measured population size [panel (a)] and environment size [panel (b)] systematically changes the exponents measured from the simplified spatial coding model. These trends from the tile model are quantified between the hippocampal spatial coding model and hippocampal data by restricting population size [panel (c)] and environment size [panel (d)] and observing the effects on the exponents measured in both hippocampal spatial coding model and hippocampal data [95% confidence intervals in both plots; for panel (c), variance is combined from temporal bootstrapping that is standard to PRG as well as permutations over subpopulations].

recent analyses of human brain data that have identified nontrivial scaling relations under PRG without invoking criticality [27]. From this perspective, heterogeneity in neural tuning may provide a robust mechanism for achieving scale invariance when coarsening neural activity without the fragility of fine-tuning to a critical point. However, the functional benefit of the power laws specifically measured via the PRG procedure remains to be demonstrated.

We have noted the similarity of PRG to the renormalization procedure used to analyze coarsening phenomena [25], where structures such as droplets merge and grow as time evolves. A crucial distinction, however, is that in coarsening the procedure reflects the intrinsic dynamics of the system, whereas for neural data, it is an externally imposed analysis with, at present, no direct counterpart in neural dynamics. This distinction underscores the need for caution when interpreting PRG outputs as signatures of dynamical criticality [19,20,28]. Our analysis highlights the role of place-field heterogeneity in generating apparent scaling, but the implications may extend beyond hippocampus: Tuning of neurons to diverse quantities is widespread in the brain, and broad distributions of tuning

properties are the norm rather than the exception. More generally, our results suggest that analyzing the distribution of tuning curves, a more direct and interpretable characterization of neural populations, should accompany any PRG analysis to assess whether observed scaling can be accounted for by known coding properties.

ACKNOWLEDGMENT

This work was supported by the Howard Hughes Medical Institute.

DATA AVAILABILITY

There are no publicly available research data or software supporting this manuscript. Requests for further information or data should be sent to the authors.

APPENDIX: TILE MODEL

Initial unit activity for the homogeneous tile model is $\sigma_n^1(x) = \Theta(\frac{l}{2} - |x - \frac{L}{N}n|)$. It is useful to define $\delta x = L/N$, the spacing between unit activities, and use $K = 2^k$ denoting the cluster size. Since the most correlated units are adjacent to one another, we can examine the statistics of a sum of adjacent units. The units grow with K in amplitude until it reaches the number of active units at a given location, N_{active}. While $1 < K < N_{\text{active}}$, we have

$$P(\sigma_n^K = m) = \begin{cases} 1 - \frac{l+(K-1)\delta x}{L}, & m = 0, \\ \frac{2\delta x}{L}, & 0 < m < K, \\ \frac{l-(K-1)\delta x}{L}, & m = K. \end{cases} \tag{A1}$$

For $K \geqslant N_{\text{active}}$,

$$P(\sigma_n^K = m) = \begin{cases} 1 - \frac{l+(K-1)\delta x}{L}, & m = 0, \\ \frac{2\delta x}{L}, & 0 < m < N_{\text{active}}, \\ \frac{l+(K-2N_{\text{active}}+1)\delta x}{L}, & m = N_{\text{active}}. \end{cases} \tag{A2}$$

The mean value $\langle \sigma_n^K \rangle_x = K\frac{l}{L}$. The probability of silence is therefore

$$P_0 = 1 - \frac{l + (K-1)\delta x}{L}. \tag{A3}$$

This quantity decreases linearly with $K = 2^k$, although an approximation of the "power-law" fit at any point can be estimated using $\beta_{\text{est}} = \frac{\partial \ln[-\ln P_0]}{\partial \ln K}|_{K=K^*}$. The variance can also be computed with different scaling relations for $K < N_{\text{active}}$ and $K > N_{\text{active}}$:

$$\text{Var}_x(\sigma_n^K) = \begin{cases} \frac{\delta x}{3L}K(1-K^2) + \frac{l}{L}(1-\frac{l}{L})K^2, & K < N_{\text{active}}, \\ -\frac{l}{3L}(N_{\text{active}}^2 - 1) + \frac{l}{L}N_{\text{active}}K - \frac{l^2}{L^2}K^2, & K \geqslant N_{\text{active}}. \end{cases} \tag{A4}$$

This is explicitly more complex than simple power-law scaling. When the number of place cells covering each position is large and the size of each place field is much smaller than the total size of the environment, then $1 \ll N_{\text{active}} \ll N$, the two regimes $K \ll N_{\text{active}}$ and $N \gg K \gg N_{\text{active}}$ are well separated, and distinct power laws are observed in each of them. Namely, for $K \ll N_{\text{active}}$, the variance scales like K^2, $\text{Var}_x(\sigma_n^K) \sim K^2 l/L$, while for $N \gg K \gg N_{\text{active}}$, it scales like K, $\text{Var}_x(\sigma_n^K) \sim K N_{\text{active}} l/L$. Thus, when K increases, the variance exponent crosses over from $\alpha = 2$ to $\alpha = 1$ [which can be observed in the green inset to Fig. 3(d)], as observed in other physical systems [29]. These idealized well-separated regimes do not seem, however, attainable with neural data, which allows for limited coarse graining only. Power-law approximations can be made using $\alpha_{\text{est}} = \frac{\partial \ln \text{Var}_x(\sigma_n^K)}{\partial \ln K}|_{K=K^*}$. Since these units are single peaked (unlike real place cells), the autocorrelation function, $A^K(\Delta x)$, goes to negative values for large distances, rendering the exponential fit inapplicable. One instructive parameter regime to compute this is $K > N_{\text{active}}$, $N_{\text{active}}\delta x \leqslant \Delta x \leqslant (K - N_{\text{active}} + 1)\delta x$, which gives

$$A^K(\Delta x) = N_{\text{active}}^2 \frac{K\delta x - \Delta x}{L} - \frac{l^2}{L^2}K^2. \tag{A5}$$

This gives a linear falloff and describes the bulk of autocorrelation decay when $K \gg N_{\text{active}}$. The characteristic length of this process is the extent of the coarse-grained unit's response, $\tilde{x} = l + (K-1)\delta x = (K + N_{\text{active}} - 1)\delta x$. A power-law estimate can be made giving $z_{\text{est}} = \frac{\partial \ln \tilde{x}}{\partial \ln K}|_{K=K^*} = \frac{K^*}{K^* + N_{\text{active}-1}}$. Another instructive example is $K < N_{\text{active}}$, $(K-1)\delta x \leqslant \Delta x \leqslant l - (K-1)\delta x$. In this case, the autocorrelation function can be calculated as

$$A^K(\Delta x) = \left[l\left(1 - \frac{l}{L}\right) - \Delta x \right] \frac{K^2}{L}. \tag{A6}$$

In this case, the characteristic length of the autocorrelation function is approximately $\tilde{x} = (1 - l/L)l$, and there is no K dependence. We did not calculate the within-cluster eigenvalue spectrum for the tile model analytically.

[1] L. P. Kadanoff, Scaling laws for Ising models near T_c, Phys. Phys. Fiz. **2**, 263 (1966).

[2] K. G. Wilson, Renormalization group and critical phenomena. I. Renormalization group and the Kadanoff scaling picture, Phys. Rev. B **4**, 3174 (1971).

[3] K. G. Wilson and J. Kogut, The renormalization group and the ϵ expansion, Phys. Rep. **12**, 75 (1974).

[4] D. J. Amit and V. Martín-Mayor, *Field Theory, the Renormalization Group, and Critical Phenomena* (World Scientific, Singapore, 2005), 3rd ed.

[5] L. Meshulam, J. L. Gauthier, C. D. Brody, D. W. Tank, and W. Bialek, Coarse-graining and hints of scaling in a population of 1000+ neurons, arXiv:1812.11904.

[6] L. Meshulam, J. L. Gauthier, C. D. Brody, D. W. Tank, and W. Bialek, Coarse graining, fixed points, and scaling in a large population of neurons, Phys. Rev. Lett. **123**, 178103 (2019).

[7] D. S. Berman, M. S. Klinger, and A. G. Stapleton, Bayesian renormalization, Mach. Learn.: Sci. Technol. **4**, 045011 (2023).

[8] E. Garuccio, M. Lalli, and D. Garlaschelli, Multiscale network renormalization: Scale-invariance without geometry, Phys. Rev. Res. **5**, 043101 (2023).

[9] J. S. Sooter, A. J. Fontenele, C. Ly, A. K. Barreiro, and W. L. Shew, Cortex deviates from criticality during action and deep sleep: A temporal renormalization group approach, bioRxiv 10.1101/2024.05.29.596499 (2024).

[10] D. J. Schwab, I. Nemenman, and P. Mehta, Zipf's law and criticality in multivariate data without fine-tuning, Phys. Rev. Lett. **113**, 068102 (2014).

[11] L. Aitchison, N. Corradi, and P. E. Latham, Zipf's law arises naturally when there are underlying, unobserved variables, PLoS Comput. Biol. **12**, e1005110 (2016).

[12] J. Touboul and A. Destexhe, Power-law statistics and universal scaling in the absence of criticality, Phys. Rev. E **95**, 012413 (2017).

[13] C. Stringer, M. Pachitariu, N. Steinmetz, M. Carandini, and K. D. Harris, High-dimensional geometry of population responses in visual cortex, Nature (London) **571**, 361 (2019).

[14] A. Faqeeh, S. Osat, F. Radicchi, and J. P. Gleeson, Emergence of power laws in noncritical neuronal systems, Phys. Rev. E **100**, 010401(R) (2019).

[15] R. J. Cubero, J. Jo, M. Marsili, Y. Roudi, and J. Song, Statistical criticality arises in most informative representations, J. Stat. Mech. (2019) 063402.

[16] M. C. Morrell, A. J. Sederberg, and I. Nemenman, Latent dynamical variables produce signatures of spatiotemporal criticality in large biological systems, Phys. Rev. Lett. **126**, 118302 (2021).

[17] V. Priesemann and O. Shriki, Can a time varying external drive give rise to apparent criticality in neural systems? PLoS Comput. Biol. **14**, e1006081 (2018).

[18] M. C. Morrell, I. Nemenman, and A. Sederberg, Neural criticality from effective latent variables, eLife **12**, RP89337 (2024).

[19] A. Ponce-Alvarez, M. L. Kringelbach, and G. Deco, Critical scaling of whole-brain resting-state dynamics, Commun. Biol. **6**, 627 (2023).

[20] G. B. Morales, S. di Santo, and M. A. Muñoz, Quasiuniversal scaling in mouse-brain neuronal activity stems from edge-of-instability critical dynamics, Proc. Natl. Acad. Sci. USA **120**, e2208998120 (2023).

[21] G. Nicoletti, S. Suweis, and A. Maritan, Scaling and criticality in a phenomenological renormalization group, Phys. Rev. Res. **2**, 023144 (2020).

[22] P. D. Rich, H.-P. Liaw, and A. K. Lee, Large environments reveal the statistical structure governing hippocampal representations, Science **345**, 814 (2014).

[23] J. S. Lee, J. J. Briguglio, J. D. Cohen, S. Romani, and A. K. Lee, The statistical structure of the hippocampal code for space as a function of time, context, and value, Cell **183**, 620 (2020).

[24] Y. Hu and H. Sompolinsky, The spectrum of covariance matrices of randomly connected recurrent neuronal networks with linear dynamics, PLoS Comput. Biol. **18**, e1010327 (2022).

[25] B. Derrida, C. Godrèche, and I. Yekutieli, Scale-invariant regimes in one-dimensional models of growing and coalescing droplets, Phys. Rev. A **44**, 6241 (1991).

[26] N. Mainali, R. Azeredo da Silveira, and Y. Burak, Universal statistics of hippocampal place fields across species and dimensionalities, Neuron **113**, 1110 (2025).

[27] D. M. Castro, E. P. Raposo, M. Copelli, and F. A. N. Santos, Interdependent scaling exponents in the human brain, Phys. Rev. Lett. **135**, 198401 (2025).

[28] P. Živadinović, F. Lombardi, D. Dupret, C. Boccara, S. Taveira, J. Ramirez-Villegas, G. Tkačik, and J. Csicsvari, The scaling behavior of hippocampal activity in sleep/rest predicts spatial memory performance, bioRxiv 10.64898/2026.03.11.711043 (2026).

[29] S. Lübeck, Violation of the Widom scaling law for effective crossover exponents, Phys. Rev. E **69**, 066101 (2004).